VER. JUN. 12, 2012
Preprint typeset using LaTeX style emulateapj v. 11/10/09



# GAS MOTION STATISTICS OF LY$\alpha$ EMITTERS AT $Z \sim 2$ USING UV AND OPTICAL EMISSION LINES ‡

TAKUYA HASHIMOTO [1], MASAMI OUCHI [2,3,4,13], KAZUHIRO SHIMASAKU [1,5], YOSHIAKI ONO [1,2], KIMIHIKO NAKAJIMA [1,3], MICHAEL RAUCH [4], JANICE LEE [4,6,13], AND SADANORI OKAMURA [1,5]

*Ver. Jun. 12, 2012*

## ABSTRACT

We present the results of Magellan/MMIRS and Keck/NIRSPEC spectroscopy for five Ly$\alpha$ emitters (LAEs) at $z = 2.2$ for which high-resolution Ly$\alpha$ spectra are available. We detect H$\alpha$ emission for all five objects and [OII], H$\beta$, and/or [OIII] emission for some, from which the systemic velocity is measured. We obtain the offset of Ly$\alpha$ line with respect to the systemic velocity, $\Delta v_{\rm Ly\alpha}$. For a sample of eight $z \sim 2-3$ LAEs without AGN from our study and the literature, we find the average offset velocity of $\Delta v_{\rm Ly\alpha} = 145^{+45}_{-23}$ km s$^{-1}$, which is significantly smaller than that of Lyman Break Galaxies (LBGs), $\Delta v_{\rm Ly\alpha} \simeq 400$ km s$^{-1}$. Since any of the LAEs with positive $\Delta v_{\rm Ly\alpha}$ has an asymmetric Ly$\alpha$ profile that cannot be explained by static gas cloud models, this average $\Delta v_{\rm Ly\alpha}$ implies that most LAEs have a gas outflow but with a systematically smaller velocity than those of LBGs. Interestingly, we find an anti-correlation between Ly$\alpha$ equivalent width (EW) and $\Delta v_{\rm Ly\alpha}$ in the compilation of the LAE and LBG samples that galaxies with stronger Ly$\alpha$ emission have smaller $\Delta v_{\rm Ly\alpha}$. Although its physical origin is unknown, this anti-correlation result would challenge the hypothesis that a strong outflow produces a large Ly$\alpha$ EW because of reduced numbers of resonant scattering through the inter-stellar medium. If LAEs at $z > 6$ have similarly small $\Delta v_{\rm Ly\alpha}$, some reionization models need to revise the amount of Ly$\alpha$ photons scattered by the inter-galactic medium.

*Subject headings:* cosmology: observations — galaxies: formation — galaxies: evolution — galaxies: high-redshift —

## 1. INTRODUCTION

Ly$\alpha$ emitters (LAEs) are objects with a large rest-frame Ly$\alpha$ equivalent width, EW(Ly$\alpha$) $\gtrsim$ 20 Å. This population is usually selected using a narrow band filter for Ly$\alpha$ emission combined with a broad band filter which measures continuum emission around Ly$\alpha$. Very recently, nearby LAEs down to $z \sim 0.2$ have also been studied with GALEX data (e.g., Cowie et al. 2011). Previous studies have revealed that most (high-$z$) LAEs are young, low-mass galaxies with small dust extinction, while some are old, massive, and dusty (Ono et al. 2010). Morphological studies have revealed that LAEs are smaller than typical high-$z$ star forming galaxies (Bond et al. 2009, 2010). Thus, LAEs are among the building block candidates in the $\Lambda$ CDM model, where smaller and less massive galaxies merge to be larger and massive ones.

Gas exchanges between galaxies and the ambient IGM, i.e., outflows and inflows, are thought to play important roles in galaxy evolution. Outflow is driven by supernovae (SNe), stellar winds from massive stars, and AGN activity. Galaxies which lost cold gas by outflow may reduce or even shutdown the subsequent star formation. In contrast, cold gas supplied by inflow may increase the star formation, especially when it comes in the form of dense, filamentary gas streams ('cold accretion'; e.g. Dekel et al. 2009). The gas exchanges will also affect the chemical evolution of galaxies and the IGM.

Outflows have been found in nearby starburst galaxies (Heckman et al. 1990), nearby ULIRGs (Martin 2005), Lyman break galaxies (LBGs) at $z \sim 2-3$ (Pettini et al. 2002; Shapley et al. 2003) and BX/BM LBGs at $z \sim 2.2$ (Steidel et al. 2010). These studies made use of the fact that FUV interstellar (IS) absorption lines, which are generated when continuum photons encounter the outflowing gas, are blue-shifted with respect to the systemic redshift which is measured by nebular emission lines such as H$\alpha$ originated from HII regions in a galaxy.

Examining if LAEs have outflows is interesting, since they are generally less massive and thus have shallower gravitational potentials. Some authors have argued the importance of outflow from less massive galaxies in chemical enrichment (e.g., Larson 1974). However, FUV continua of LAEs are too faint for metal absorption lines to be reliably measured with current facilities.

However, Ly$\alpha$ is also used to probe the gas kinematics. Ly$\alpha$ line is known to have complicated profiles due to its resonant nature. Many theoretical and observational studies have shown that if there is an outflow, the peak of the Ly$\alpha$ profile is redshifted with respect to the systemic redshift (e.g., Verhamme et al. 2006; Steidel et al. 2010), giving a positive Ly$\alpha$ offset velocity, $\Delta v_{\rm Ly\alpha}$. This is due to the fact that in the outflow situation, back-scattered

thashimoto _at_ astron.s.u-tokyo.ac.jp
[1] Department of Astronomy, Graduate School of Science, The University of Tokyo, Tokyo 113-0033, Japan
[2] Institute for Cosmic Ray Research, The University of Tokyo, 5-1-5 Kashiwanoha, Kashiwa, Chiba 277-8582, Japan
[3] Kavli Institute for the Physics and Mathematics of the Universe (WPI) , The University of Tokyo, 5-1-5 Kashiwanoha, Kashiwa, Chiba 277-8583, Japan
[4] Observatories of the Carnegie Institution of Washington, 813 Santa Barbara Street, Pasadena, CA 91101, USA
[5] Research Center for the Early Universe, Graduate School of Science, The University of Tokyo, Tokyo 113-0033, Japan
[6] Space Telescope Science Institute, Baltimore, MD, USA
[13] Carnegie Fellow

‡ Based on data collected at the Subaru Telescope, which is operated by the National Astronomical Observatory of Japan.

(i.e., redshifted) Ly$\alpha$ toward the observer can easily escape the foreground gas with much reduced numbers of scattering. It is very difficult to obtain high-resolution nebular emission lines because they are faint compared with strong sky emission. Prior to our study, only four LAEs have both a high-resolution Ly$\alpha$ spectrum and a nebular line: two from McLinden et al. (2011) and two from Finkelstein et al. (2011). McLinden et al.'s two objects have $\Delta v_{\rm Ly\alpha} = 284 \pm 13$ and $142 \pm 13$ km s$^{-1}$ and Finkelstein's objects have $\Delta v_{\rm Ly\alpha} = 36 \pm 35$ and $162 \pm 37$ km s$^{-1}$. The fact that three out of the four have $\Delta v_{\rm Ly\alpha} > 0$ suggests that outflow is common to LAEs, but due to its small sample size, there has been no statistical discussion on the gas motions of LAEs.

To answer the fundamental question "why LAEs have strong Ly$\alpha$ emission" is crucial for understanding physical nature of LAEs. Some studies have shown that outflow is essential for Ly$\alpha$ photons to escape from galaxies (e.g., Kunth et al. 1998) because the chance of resonant scattering is reduced in the outflow situation. Indeed, Verhamme et al. (2006, 2008) have carried out Ly$\alpha$ radiative transfer simulations, and claimed that expanding shell models can account for observed Ly$\alpha$ spectral profiles of LBGs. Thus, the Ly$\alpha$ radiative transfer mechanism of high-$z$ galaxies has been relatively well understood in the context of outflow, however, the reason why LAEs have strong Ly$\alpha$ emission is still an open question. This is because only a small number of LAEs have both a high-resolution Ly$\alpha$ spectrum and a high-resolution nebular line spectrum both of which are essential for testing the models.

Addressing these questions, we are conducting near infrared spectroscopy for optically confirmed LAEs at $z \simeq 2.2$ promising for detecting nebular emission lines. This redshift is unique since we can simultaneously observe Ly$\alpha$ and nebular lines (e.g, [OII], H$\beta$, [OIII], and H$\alpha$) from the ground. Furthermore, we can compare the kinematics and Ly$\alpha$ radiative transfer of LAEs with those of brighter and more massive galaxies at similar redshifts, e.g. LBGs, obtained by previous studies.

We successfully detect nebular emission lines and measure $\Delta v_{\rm Ly\alpha}$ for all of our spectroscopic targets. We also derive physical quantities such as EW(Ly$\alpha$), Ly$\alpha$ escape fraction ($f_{\rm esc}^{\rm Ly\alpha}$), star-formation rate (SFR), mass, and the size of the star-forming region from the spectral data and photometric data (SED fitting). Using these quantities, we discuss the gas kinematics of LAEs and give implications on the physical origin of the strong Ly$\alpha$ emission.

This paper is organized as follows. Our near infrared spectroscopy is described in §2. After performing SED fitting in §3, we derive $\Delta v_{\rm Ly\alpha}$ and several observational quantities for our LAEs in §4. Discussion in the context of outflow and Ly$\alpha$ radiative transfer is given §5, followed by conclusions in §6. Throughout this paper, magnitudes are given in the AB system (Oke & Gunn 1983), and we assume a ΛCDM cosmology with $\Omega_m = 0.3$, $\Omega_\Lambda = 0.7$ and $H_0 = 70$ km s$^{-1}$ Mpc$^{-1}$.

## 2. SPECTROSCOPIC DATA

### 2.1. *Targets of our NIR Spectroscopy*

Our targets for near infrared spectroscopy are selected from samples of $z \simeq 2.2$ LAEs in the COSMOS and the Chandra Deep Field South (hereafter CDFS) constructed in the same manner as Nakajima et al. (2012) (see K. Nakajima et al. in preparation). These LAE samples are based on narrow-band (NB387) imaging with Subaru/Suprime-Cam, supplemented by public broad-band data. Our LAEs have been selected by imposing the following color criteria:

$$u^* - NB387 > 0.5 \ \& \ B - NB387 > 0.2 \ \text{(COSMOS)} \quad (1)$$

$$U - NB387 > 0.8 \ \& \ B - NB387 > 0.2 \ \text{(CDFS)}. \quad (2)$$

The COSMOS (CDFS) sample contains 619 (1,108) LAEs with EW$\gtrsim$30Å down to $NB387 = 26.1$ (26.4). Among them, two objects in the CDFS sample (CDFS-3865, CDFS-6482) and three in the COSMOS sample (COSMOS-13636, COSMOS-30679, COSMOS-43982) have a high-quality Magellan/MagE spectrum of Ly$\alpha$ (M. Rauch et al. in preparation). These five objects are our targets of NIR spectroscopy. They have typical NB387 excesses among the whole LAE sample in each field while having relatively bright NB387 magnitudes.

### 2.2. *Near Infrared Spectroscopy*

We observed the two CDFS objects on 2010 October 21 with Magellan/MMIRS using the HK grism covering 1.254 – 2.45$\mu$m. The total exposure time was 10800s for each object. The slit width was 0.″5 resulting in $R \equiv \lambda/\Delta\lambda \sim 1120$. A two-point dither pattern (A1,B1,A2,B2,A3,B3,...) was adopted. The A0V standard star HIP-16904 was also observed. The sky was clear through our observation run, with seeing sizes of 0.″5 – 0.″9.

The three COSMOS objects were observed on 2011 February 10 and 11 with Keck-II/NIRSPEC. COSMOS-30679 was observed with NIRSPEC-3 ($J$ band; 1.15 – 1.36$\mu$m), NIRSPEC-5 ($H$ band; 1.48 – 1.76$\mu$m), and NIRSPEC-6 ($K$ band; 2.2 – 2.43$\mu$m) filters in the low-resolution mode, while COSMOS-13636 and COSMOS-30679 were observed with the $K$ band alone. Furthermore, we observed CDFS-3865 with the $J$ band targeting [OII] $\lambda\lambda 3726, 3729$. Total exposure times are shown in Table 1. The slit width was 0.″76 for all three objects, corresponding to $R \sim 1500$ for both grisms. A two-point dither pattern was adopted. We used the invisible acquisition mode because of the faintness of our targets. The A0V standard star HIP-13917 was also observed. The sky was clear in our observing nights, with seeing sizes of 0.″6 – 0.″9. A summary of the spectroscopic observations is given in Table 1.

### 2.3. *Data Reduction*

We reduced the MMIRS data using IRAF tasks and the COSMOS package which is the standard reduction pipeline for Magellan/IMACS. The MMIRS detector is read out non-destructively during a single exposure, and individual read-outs are stored as separate extensions in a FITS file through which we know whether and when a particular pixel is saturated. Bias subtraction and flat fielding were processed for each read-out using IRAF `mscred` package to treat data of this format. Then we ran `mmfixen` package which takes advantage of its sampling. This essentially fits a line to different values for a given pixel in each readout, and outputs the slope of this linear fit to the final collapsed image. Wavelength calibration and distortion correction were processed for

TABLE 1
Summary of our observations

| Object | $\alpha$(J2000) | $\delta$(J2000) | $z$(Ly$\alpha$) | $L$(Ly$\alpha$) ($10^{42}$ erg s$^{-1}$) | Date | $t_{exp}$ (s) |
|---|---|---|---|---|---|---|
| (1) | (2) | (3) | (4) | (5) | (6) | (7) |
| CDFS-3865 | 03:32:32.31 | -28:00:52.20 | $2.17507^{+0.00104}_{-0.00004}$ | $29.8 \pm 4.9$ | 2010 Oct 21 | 5100(J), 10800(HK) |
| CDFS-6482 | 03:32:49.34 | -27:59:52.35 | $2.20610^{+0.00049}_{-0.00002}$ | $15.4 \pm 4.3$ | 2010 Oct 21 | 10800(HK) |
| COSMOS-13636 | 09:59:59.38 | +02:08:38.36 | $2.16229 \pm 0.00008$ | $11.3 \pm 0.5$ | 2011 Feb 10 | 5400(K) |
| COSMOS-30679 | 10:00:29.81 | +02:18:49.00 | $2.20046 \pm 0.00008$ | $6.9 \pm 0.5$ | 2011 Feb 10 | 5400(J), 7200(H), 6300(K) |
| COSMOS-43982 | 09:59:54.39 | +02:26:29.96 | $2.19396 \pm 0.00008$ | – | 2011 Feb 10 | 3600(K) |

Notes. (1) Object ID; (2)-(3) RA and decl.; (4) Redshift of Ly$\alpha$ emission; (5) Ly$\alpha$ luminosity derived from narrow and broad-band photometry; (6) Date of observations; (7) Exposure time for a filter shown in parentheses.

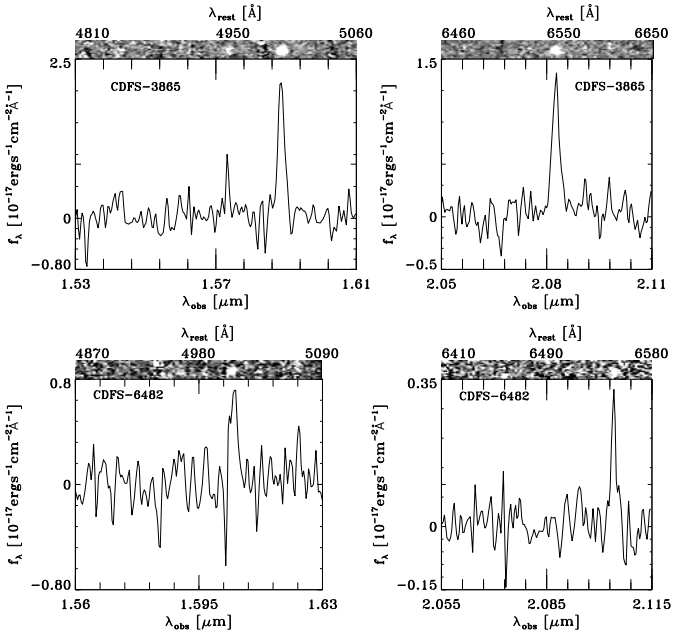


Fig. 1.— Reduced 1D+2D spectra of CDFS objects, CDFS-3865 (top) and CDFS-6482 (bottom).

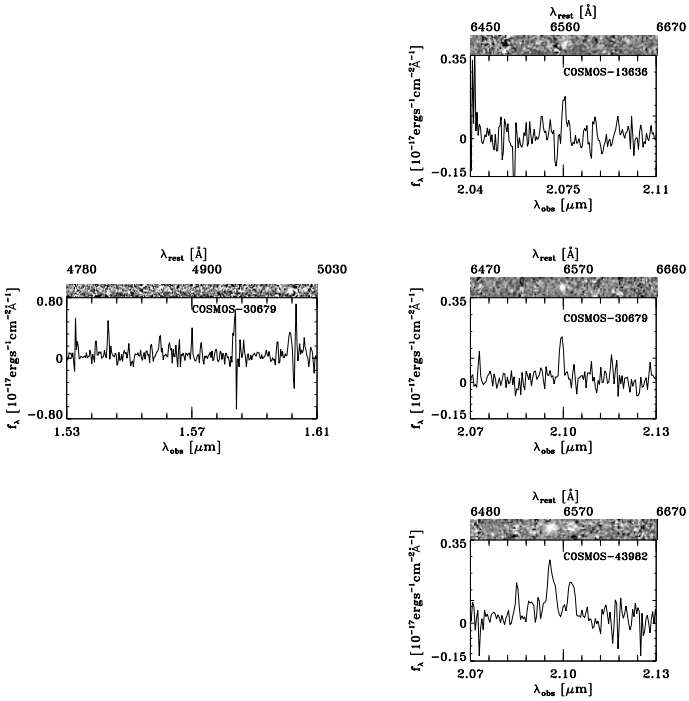


Fig. 2.— Reduced 1D+2D spectra of COSMOS objects, COSMOS-13636 (top), COSMOS-30679 (middle), and COSMOS-43982 (bottom). $H$-band data is taken only for COSMOS-30679.

each frame using COSMOS package. Although we obtained arc lamp calibration images, we used OH lines for wavelength calibration. We then performed the following operation to remove sky background: C1 = B1 - (A1 + A2)/2, C2 = B2 - (A2 + A3)/2. After this operation, we ran `subsky` in COSMOS package [9] on each frame to remove residual sky lines. Resultant frames ($C1, C2$,...) are then stacked to have a final 2D frame using `sumspec-2d` and e`xtract-2dspec` in COSMOS package. 1D spectrum extraction was carried out using `apall` in IRAF. The telluric absorption correction and flux calibration were conducted using the standard star frames. The flux-calibrated 1D spectra of the two objects are shown in Figure 1. We reduced the NIRSPEC data using mainly IRAF tasks. Details of the reduction procedure is described in K. Nakajima et al. (in preparation). The flux-calibrated 1D spectra of the three objects are shown in Figure 2.

### 2.4. *Emission Line Detections and Measurements*

We determine a line to be detected, if there exists an emission line above the $3\sigma$ sky noise around the wavelength expected from the Ly$\alpha$ redshift, where sky noise is calculated from the spectrum within 100 Å from the line wavelength. Table 2 summarizes the line detections. For each detected line, we fit a Gaussian function to calculate its central wavelength, FWHM, and flux. The central wavelength is then converted into the vacuum wavelength after correction for the heliocentric motion of the earth [10], and is adopted for the systemic redshift of the object. For the four objects with multiple line detections, we confirm that the redshifts of the lines agree within $1\sigma$ errors, and adopt their weighted mean for the systemic redshift. [Oii] is not used in the redshift measurement because the 3726/3729 doublet is not resolved in our spectra. The H$\beta$ line for CDFS-3865 is not used, either, because of the low $S/N$ ratio. We also derive $1\sigma$ upper limits of fluxes for all undetected lines. The emission line measurements are summarized in Table 2.

### 2.5. *Checking the presence of AGNs*

We examine whether our objects host an AGN in three ways. First, we compare the sky coordinates of the ob-

[9] This uses the Kelson procedure (cf, Kelson 2003).

[10] http://fuse.pha.jhu.edu/support/tools/vlsr.html

TABLE 2
Emission Line Properties

| Object | Line | $\lambda_{\rm rest}$ (Å) | $\lambda_{\rm obs}$ (Å) | $\lambda_{\rm corr.}$ (Å) | z | S/N | Insuturment |
|---|---|---|---|---|---|---|---|
| (1) | (2) | (3) | (4) | (5) | (6) | (7) | (8) |
| CDFS-3865 | [OII] | 3727.00 | -[a] | -[a] | -[a] | 6.0 | NIRSPEC |
| | H$\beta$ | 4861.33 | $15418.9 \pm 4.0$ | 15418.3 | $2.17162 \pm 0.00083$ | 3.2 | MMIRS |
| | [OIII] | 4958.91 | $15735.8 \pm 3.5$ | 15735.1 | $2.17310 \pm 0.00071$ | 5.4 | MMIRS |
| | [OIII] | 5006.84 | $15887.1 \pm 1.5$ | 15886.4 | $2.17294 \pm 0.00030$ | 15.3 | MMIRS |
| | H$\alpha$ | 6562.85 | $20825.8 \pm 1.7$ | 20824.9 | $2.17315 \pm 0.00026$ | 16.0 | MMIRS |
| | [NII] | 6583.45 | - | - | - | $< 1$ | MMIRS |
| CDFS-6482 | H$\beta$ | 4861.33 | - | - | - | $< 1$ | MMIRS |
| | [OIII] | 4958.91 | - | - | - | $< 1$ | MMIRS |
| | [OIII] | 5006.84 | $16048.3 \pm 3.8$ | 16047.63 | $2.205144 \pm 0.00076$ | 8.8 | MMIRS |
| | H$\alpha$ | 6562.85 | $21036.9 \pm 1.9$ | 21036.02 | $2.205317 \pm 0.00029$ | 5.6 | MMIRS |
| | [NII] | 6583.45 | - | - | - | $< 1$ | MMIRS |
| COSMOS-13636 | H$\alpha$ | 6562.85 | $20753.5 \pm 1.0$ | 20752.36 | $2.16210 \pm 0.00015$ | 7.1 | NIRSPEC |
| | [NII] | 6583.45 | - | - | - | $< 1$ | NIRSPEC |
| COSMOS-30679 | [OII] | 3727.00 | -[a] | -[a] | -[a] | 4.6 | NIRSPEC |
| | H$\beta$ | 4861.33 | - | - | - | -[b] | NIRSPEC |
| | [OIII] | 4958.91 | - | - | - | -[b] | NIRSPEC |
| | [OIII] | 5006.84 | $16013.8 \pm 1.2$ | 16013.62 | $2.19835 \pm 0.00024$ | 10.0 | NIRSPEC |
| | H$\alpha$ | 6562.85 | $20993.7 \pm 1.3$ | 20993.48 | $2.19884 \pm 0.00019$ | 11.5 | NIRSPEC |
| | [NII] | 6583.45 | - | - | - | $<1$ | NIRSPEC |
| COSMOS-43982 | H$\alpha$ | 6562.85 | $20958.50 \pm 1.2$ | 20958.26 | $2.19347 \pm 0.00018$ | 11.4 | NIRSPEC |
| | [NII] | 6583.45 | $21026.20 \pm 2.1$ | 21025.96 | $2.19376 \pm 0.00032$ | 7.1 | NIRSPEC |

Note. — The symbol "-" indicates that the line is not detected. The weighted mean redshifts are $2.17306 \pm 0.00019$ (CDFS-3865), $2.20530 \pm 0.00027$ (CDFS-6482), $2.19865 \pm 0.00015$ (COSMOS-30679) and $2.19354 \pm 0.00016$ (COSMOS-43982). (1) Object ID; (2)-(3) Line name and its rest frame wavelength; (4) Observed wavelength of the line; (5) Wavelength of the line corrected for the LSR motion; (6) Redshift; (7) Signal to noise ratio of the line detection; (8) Instrument used for the line detection.

[a] [OII] redshift is not shown because it is not reliably measured.

[b] $S/N$ upper limit is not shown because the line is contaminated by a strong OH line.

jects with those in deep archival X-ray and radio catalogues, [11] to find no counterpart to any of them.

Second, we look for three high ionization state lines typical of AGNs, CIV$\lambda$1549, HeII$\lambda$1640, and CIII]$\lambda$1909, in the spectra, and detect none of them.

Finally and most importantly, we apply the BPT diagnostic diagram (Baldwin et al. 1981) to our objects, as shown in Figure 3. The solid curve in Figure 3 shows the boundary between star-forming galaxies and AGNs proposed by Kewley et al. (2001) using photoionization models, while the dotted curve is the boundary empirically defined by SDSS objects (Kauffmann et al. 2003). In both cases, star-forming galaxies fall below the curve.

None of our objects but CDFS-3865 has detections of all four lines necessary for the BPT diagram. Thus, as shown in Figure 3, any objects logically have a possibility of being in the AGN regime. However, we conclude from the following discussion that all but COSMOS-43982 are star-forming galaxies. CDFS-3865 falls below the curves, indicating this is a starburst galaxy. CDFS-6482 have relatively high [OIII] / H$\beta$ values (lower limit), but [NII]/H$\alpha$ is not so high. This high [OIII] / H$\beta$ ratio may not be due to the presence of AGN but due to a higher gas temperature of the HII region, as has been pointed out for some high-redshift star-forming galaxies (Erb et al. 2006a). Indeed, there are few local AGN distributed around the positions of this object. Finkelstein et al. (2008) have also classified a similar object to ours as a star-forming galaxy (yellow circle in Figure 3). A similar argument is made for COSMOS-13636 and COSMOS-30679 whose [NII]/H$\alpha$ ratios are also modest. In contrast, COSMOS-43982 has a very high [NII]/H$\alpha$ ratio. Because we infer that this object is more likely to be an AGN than a star-forming galaxy, we do not use this object in the following discussion.

## 3. SED FITTING

We perform SED fitting to our objects to derive dust extinction, SFR, and stellar mass. The procedure of the SED fitting is the same as that of Ono et al. (2010). For the CDFS objects, we use 12 banpasses: $B, V, R, I, z, J, H, K$ data from MUSYC public data release [12] (Cardamone et al. 2010), and *Spitzer*/IRAC 3.6, 4.5, 5.8, and 8.0 $\mu$m photometry from the *Spitzer* legacy survey of the UDS field. For the COSMOS objects, we use 11 bandpasses: $B, V, r^{'}, i^{'}$, and $z^{'}$ data taken with Subaru/Suprime-Cam, $J$ data taken with UKIRT/WFCAM, $K_s$ data taken with CFHT/WIRCAM (McCracken et al. 2010), and *Spitzer*/IRAC 3.6, 4.5, 5.8, and 8.0 $\mu$m photometry from the *Spitzer* legacy survey of the UDS field. We use neither $u^*/U$ nor NB387-band photometry, since the photometry of these bands are contaminated by the IGM absorption and/or Ly$\alpha$ emission. Tables 3 and 4 summarize the broadband photometry of our objects. Basically, the uncertainties in the opti-

[11] CDFS http://www2.astro.psu.edu/users/niel/cdfs/cdfs-chandra.html
COSMOS http://irsa.ipac.caltech.edu/data/COSMOS/

[12] http://www.astro.yale.edu/MUSYC/

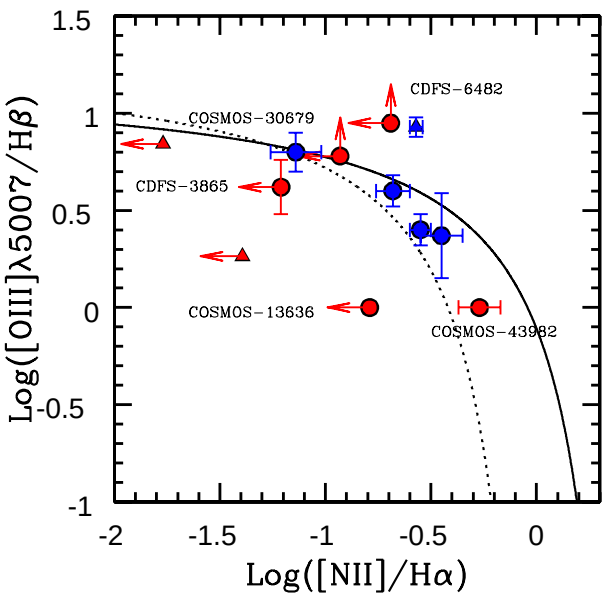


FIG. 3.— BPT diagram. The solid curve represents the boundary between star-forming galaxies and AGN proposed by Kewley et al. (2001), while the dotted curve is the boundary empirically defined by SDSS objects (Kauffmann et al. 2003). Red circles denote our LAEs. For the purpose of display, COSMOS-13636 and COSMOS-43982, whose [OIII] / H$\beta$ is not constrained, are placed at log([OIII] / H$\beta$) = 0.0. Red triangles are two $z \sim 2.3$ LAEs of Finkelstein et al. (2011). Blue circles show four $z \sim 2.2$ LBGs of Erb et al. (2006a). Blue triangle shows the lensed LBG at $z = 2.73$ (Finkelstein et al. 2009).

cal photometry include both photometric errors and systematic errors associated with aperture correction and photometric calibration.

We use the stellar population synthesis model of GALAXEV (Bruzual & Charlot 2003) including nebular emission (Schaerer & de Barros 2009), and adopt Salpeter initial mass function (Salpeter 1955). Because LAEs are metal poor star-forming galaxies, we choose constant star formation history and the metallicity of $Z/Z_{\odot} = 0.2$. We use Calzetti's law (Calzetti et al. 2000) for the stellar continuum extinction of $E(B-V)_*$. We apply Madau (1995)'s prescription to correct for the IGM attenuation; at $z \simeq 2.2$, continuum photons shortward of Ly$\alpha$ are absorbed by 18 %. Figure 4 shows the best-fit model spectra with the observed flux densities for individual objects. The properties derived from SED fitting are listed in Table 5. Because the continuum emission of COSMOS-30679 is blended with a foreground object, we deblend the source with GALFIT (Peng et al. 2002; see K. Nakajima et al. in preparation for more details). We present both photometry data of the blended and deblended sources in Table 4. We use the photometry of deblended source for our SED fitting.

## 4. PHYSICAL QUANTITIES OF OUR LAES

### 4.1. *Velocity Offset Between Ly$\alpha$ and Nebular Lines*

We calculate a quantity called the velocity offset of the Ly$\alpha$ line:

$$\Delta v_{\mathrm{Ly}\alpha} = c\frac{z_{\mathrm{Ly}\alpha} - z_{\mathrm{sys}}}{1 + z_{\mathrm{sys}}}, \quad (3)$$

where $z_{\mathrm{Ly}\alpha}$ is the redshift of Ly$\alpha$ emission and $z_{\mathrm{sys}}$ is the systemic redshift listed in Table 2.

We show the Ly$\alpha$ and H$\alpha$ profiles of our LAEs in Figure 5. Most objects have a Ly$\alpha$ profile which is asymmetric and/or double peaked. Similar to previous studies (Steidel et al. 2010; Yang et al. 2011), we define $z_{\mathrm{Ly}\alpha}$ to be the redshift corresponding to the wavelength at the highest peak. The peak wavelength is determined as follows. First, we roughly constrain the peak position by eye. For the CDFS objects, we cannot identify where is the highest peak, since the second peak is within the $1\sigma$ error in the height of the first peak. In these cases, we regard both as peak candidates and include their wavelength difference as the error in $z_{\mathrm{Ly}\alpha}$ (as listed in Table 1). Then, we fit a Gaussian to the profile only around the peak to derive the peak wavelength, in order to avoid systematic effects due to the asymmetric profile. The Ly$\alpha$ line of COSMOS-30679 is partly contaminated by a cosmic ray. It is, however, unlikely that there is a true peak under the cosmic ray. Even if there is a flux peak just under the cosmic ray, our discussion remains unchanged.

We find $\Delta v_{\mathrm{Ly}\alpha} = 190^{+99}_{-18}$ km s$^{-1}$ (CDFS-3865), $75^{+52}_{-25}$ km s$^{-1}$ (CDFS-6482), $18 \pm 16$ km s$^{-1}$ (COSMOS-13636), and $170 \pm 16$ km s$^{-1}$ (COSMOS-30679). Thus, our LAEs have positive $\Delta v_{\mathrm{Ly}\alpha}$ beyond the 1 sigma uncertainties.

There are four LAEs in the literature which have both a Ly$\alpha$ spectrum and a systemic-velocity measurement from a nebular line: two from McLinden et al. (2011) and two from Finkelstein et al. (2011). The $\Delta v_{\mathrm{Ly}\alpha}$ of these four LAEs ranges from 0 to $\sim$ 300km s$^{-1}$, which is very similar to our $\Delta v_{\mathrm{Ly}\alpha}$ measurements. We combine these four LAEs with our four to construct a sample of eight LAEs at $z = 2-3$, and investigate average physical properties of LAEs using them. Figure 6 presents the histogram of $\Delta v_{\mathrm{Ly}\alpha}$ for the eight LAEs. Most LAEs have a relatively small $\Delta v_{\mathrm{Ly}\alpha}$ of $0-200$ km $^{-1}$. The average of the eight is $\Delta v_{\mathrm{Ly}\alpha} = 145^{+45}_{-23}$ km s$^{-1}$, which is systematically smaller, by $\sim 200-300$ km s$^{-1}$, than that of LBGs, $\Delta v_{\mathrm{Ly}\alpha} \simeq 400$ km s$^{-1}$, (Pettini et al. 2002; Shapley et al. 2003; Steidel et al. 2010; Rakic et al. 2011) at a similar redshift of $z = 2-3$.

Figure 7 shows $\Delta v_{\mathrm{Ly}\alpha}$ as a function of the rest-frame Ly$\alpha$ EW, where data for LBGs are also included (Reddy et al. 2008; Steidel et al. 2010) in order to cover a wide baseline of EW, $0-200$ Å. We fit a linear function to the data points (solid line in Figure 7), and find an anti-correlation between $\Delta v_{\mathrm{Ly}\alpha}$ and Ly$\alpha$ EW; galaxies with stronger Ly$\alpha$ emission have a smaller $\Delta v_{\mathrm{Ly}\alpha}$.

### 4.2. *Dust Extinction*

Since the spectra of CDFS-3865 and CDFS-6482 cover H$\beta$ as well as H$\alpha$, [13], we obtain Balmer decrement (H$\alpha$/H$\beta$) measurements to constrain color excess of nebular emission, $E(B-V)_{gas}$. The Balmer decrement values are measured to be $2.96 \pm 0.87$ and $> 1.74$ (using H$\beta$'s $2\sigma$ limit) for CDFS-3865 and CDFS-6482, respectively. Adopting the intrinsic ratio of 2.86 (Osterbrock 1989) and Calzetti et al. (2000)'s extinction law, we find $E(B-V)_{gas} = 0.03^{+0.27}_{-0.03}$ for CDFS-3865 and $E(B-V)_{gas} > 0$ for CDFS-6482.

[13] COSMOS-30679 also has H$\beta$ data, but the line is heavily contaminated by a sky emission line.

TABLE 3
Broadband Photometry of our Sample (CDFS)

| Object | $B$ | $V$ | $R$ | $I$ | $z$ | $J$ | $H$ | $K$ | [3.6] | [4.5] | [5.8] | [8.0] |
|---|---|---|---|---|---|---|---|---|---|---|---|---|
| CDFS-3865 | 23.01 | 22.94 | 22.92 | 23.14 | 22.93 | 22.73 | 22.27 | 22.38 | 22.82 | 22.82 | 22.51 | 23.00 |
| | (28.32) | (27.85) | (27.82) | (26.14) | (25.64) | (24.57) | (24.57) | (23.97) | (26.23) | (25.68) | (23.66) | (23.43) |
| CDFS-6482 | 23.93 | 23.87 | 23.78 | 23.95 | 23.67 | 23.50 | 23.36 | 23.07 | 22.88 | 22.83 | 23.34 | 99.99 |
| | (28.32) | (27.85) | (27.82) | (26.14) | (25.64) | (24.57) | (24.57) | (23.97) | (26.23) | (25.68) | (23.66) | (23.43) |

Note. — All magnitudes are total magnitudes. 99.99 mag indicates a negative flux density. A magnitude in parenthesis is $1\sigma$ uncertainty.

TABLE 4
Broadband Photometry of our Sample (COSMOS)

| Object | $B$ | $V$ | $r'$ | $i'$ | $z'$ | $J$ | $K_s$ | [3.6] | [4.5] | [5.8] | [8.0] |
|---|---|---|---|---|---|---|---|---|---|---|---|
| COSMOS-13636 | 24.43 | 24.21 | 24.35 | 24.19 | 24.24 | 23.10 | 23.43 | 24.10 | 23.75 | 99.99 | 99.99 |
| | (29.13) | (28.18) | (28.33) | (27.87) | (26.89) | (24.17) | (24.84) | (25.05) | (24.25) | (21.90) | (20.63) |
| COSMOS-30679[a] | 24.05 | 23.12 | 22.91 | 22.46 | 22.33 | 21.15 | 21.83 | 22.12 | 22.57 | 99.99 | 23.06 |
| | (29.13) | (28.18) | (28.33) | (27.87) | (26.89) | (24.17) | (24.84) | (25.05) | (24.25) | (21.90) | (20.63) |
| COSMOS-30679[b] | 24.76 | 23.82 | 24.44 | 24.09 | 23.49 | 22.31 | 23.29 | - | - | - | - |
| | (28.76) | (26.24) | (25.79) | (25.34) | (24.85) | (23.68) | (24.63) | ( - ) | ( - ) | ( - ) | ( - ) |

Note. — All magnitudes are total magnitudes. 99.99 mag indicates a negative flux density. A magnitude in parenthesis is a $1\sigma$ uncertainty.
[a] Before the foreground source debelending.
[b] After the foreground source debelending.

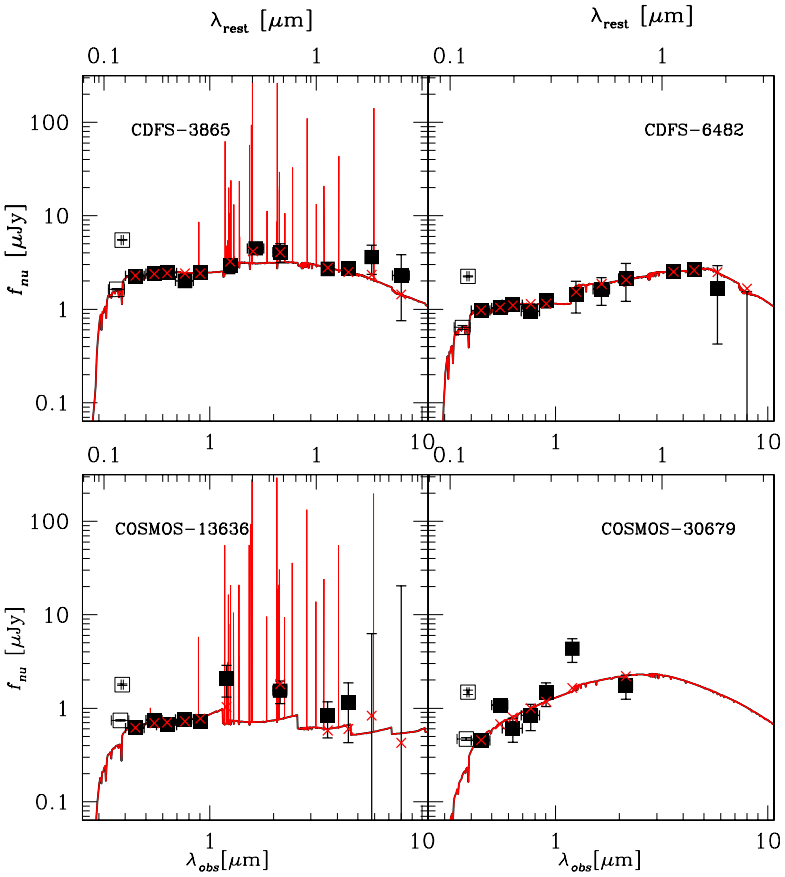


Fig. 4.— Upper (lower) panel shows the SEDs of CDFS (COSMOS) objects. Filled squares denote the photometry points used for our SED fitting, while open squares are those omitted in our SED fitting due to the contamination of Ly$\alpha$ emission and IGM absorption. The red lines present the best-fit model spectra, and the red crosses correspond to the flux densities expected from the best-fit models.

The color excess of the stellar continuum, $E(B-V)_*$, from the SED fitting is $0.185^{+0.009}_{-0.009}$ (CDFS-

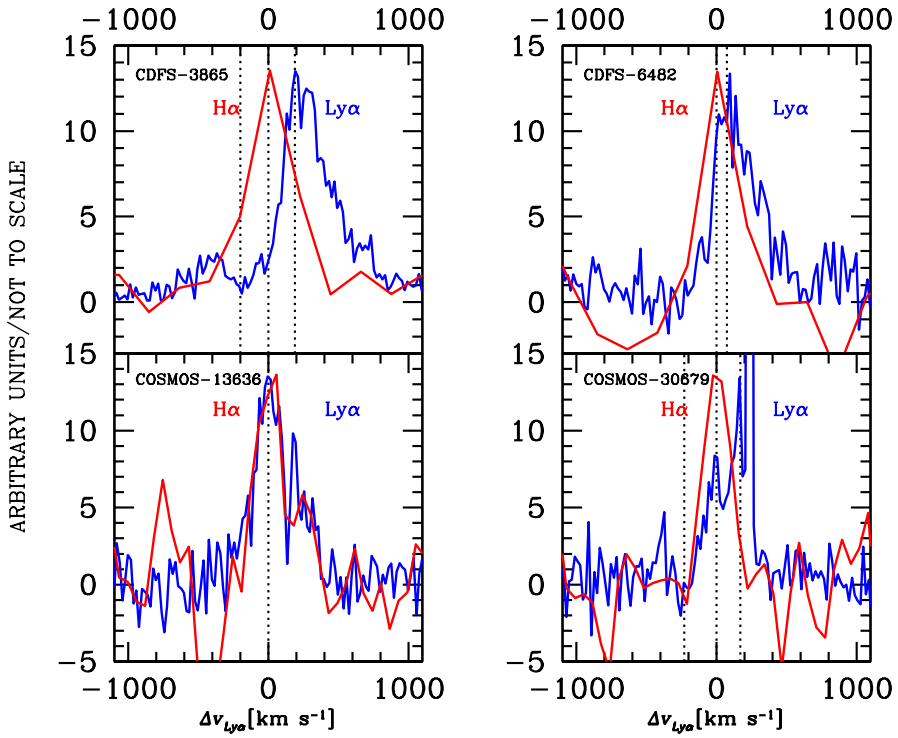


FIG. 5.— Comparison between Lyα (blue line) and Hα (red line) emission profiles. *Top left:* CDFS−3865 with $\Delta v_{\mathrm{Ly}\alpha} = 190^{+99}_{-18}$ $kms^{-1}$. The left, center, and right dotted lines indicate the trough redshift, the systemic redshift, and the Lyα redshift, respectively. *Top right:* CDFS−6482 with $\Delta v_{\mathrm{Ly}\alpha} = 75^{+52}_{-25}$ $kms^{-1}$. The left and right dotted lines show the systemic redshift and the Lyα redshift, respectively. *Bottom left:* COSMOS-13636 with $\Delta v_{\mathrm{Ly}\alpha} = 18 \pm 16$ $kms^{-1}$. The dotted line represents the systemic redshift and the Lyα redshift, *Bottom right:* COSMOS-30679 with $\Delta v_{\mathrm{Ly}\alpha} = 170 \pm 16$ $kms^{-1}$. Three dotted lines are the same as those of the top-left panel, but for COSMOS-30679.

TABLE 5
RESULTS OF SED FITTING

| Object | $E(B-V)_*$ | $SFR_{SED}$ ($M_\odot$ yr$^{-1}$) | $M_*$ ($10^9$ $M_\odot$) | $\chi^2$ |
|---|---|---|---|---|
| (1) | (2) | (3) | (4) | (5) |
| CDFS-3865 | $0.185^{+0.009}_{-0.009}$ | $312^{+41}_{-43}$ | $3.18^{+0.21}_{-0.13}$ | 17 |
| CDFS-6482 | $0.185^{+0.026}_{-0.018}$ | $83^{+34}_{-18}$ | $5.30^{+1.18}_{-0.80}$ | 5 |
| COSMOS-13636 | $0.273^{+0.018}_{-0.079}$ | $1311^{+17574}_{-1244}$ | $1.99^{+0.39}_{-1.06}$ | 21 |
| COSMOS-30679 | $0.528^{+0.026}_{-0.026}$ | $7510^{+201248}_{-3097}$ | $19.75^{+6.53}_{-5.80}$ | 20 |

Notes. Stellar metallicity is fixed to 0.2 $Z_\odot$.
(1) Object ID; (2) Dust extinction; (3) Star formation rate; (4) Stellar mass; (5) $\chi^2$ of the fitting.

3865), $0.185^{+0.026}_{-0.018}$ (CDFS-6482), $0.273^{+0.018}_{-0.079}$ (COSMOS-13636), and $0.528^{+0.026}_{-0.026}$ (COSMOS-30679) for the Calzetti et al. (2000)'s extinction law. The $E(B-V)_*$ values of our four LAEs are comparable to those of relatively faint (stacked) LAEs at $z \sim 2$; $E(B-V)_* = 0.27^{+0.01}_{-0.03}$ (Nakajima et al. 2012), $E(B-V)_* = 0.22^{+0.06}_{-0.13}$ (Guaita et al. 2011). On the other hand, the $E(B-V)_*$ values of our LAEs are larger than those of the two bright LAEs observed by Finkelstein et al. (2011) (HPS194 and HPS256), $E(B-V)_* = 0.09 \pm 0.05$ and $E(B-V)_* = 0.10 \pm 0.10$. Since our objects are as bright as Finkelstein et al. (2011)'s LAEs, this difference may indicate that LAEs at $z \sim 2$ have a wide range of dust extinction even at the same Lyα luminosity range.

Figure 8 plots $E(B-V)_*$ vs. $E(B-V)_{gas}$ for our objects. CDFS-3865 has the $E(B-V)_{gas}$ measurement from Balmer decrement comparable to the $E(B-V)_*$

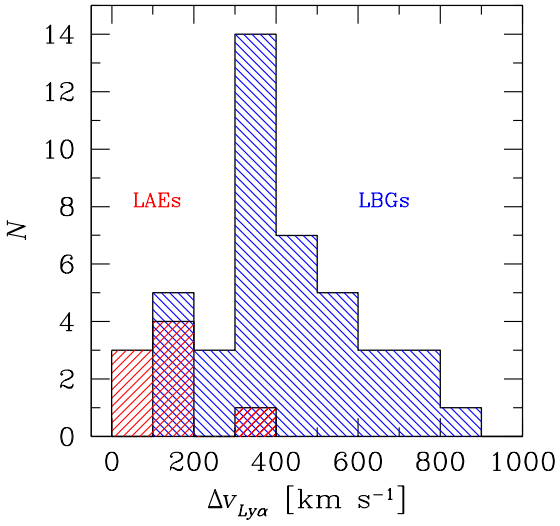


FIG. 6.— Histograms of $\Delta v_{\mathrm{Ly}\alpha}$. The red histogram shows the eight LAEs, and the blue histogram denotes 41 LBGs given by Steidel et al. (2010). LAEs have a generally smaller $\Delta v_{\mathrm{Ly}\alpha}$ than LBGs.

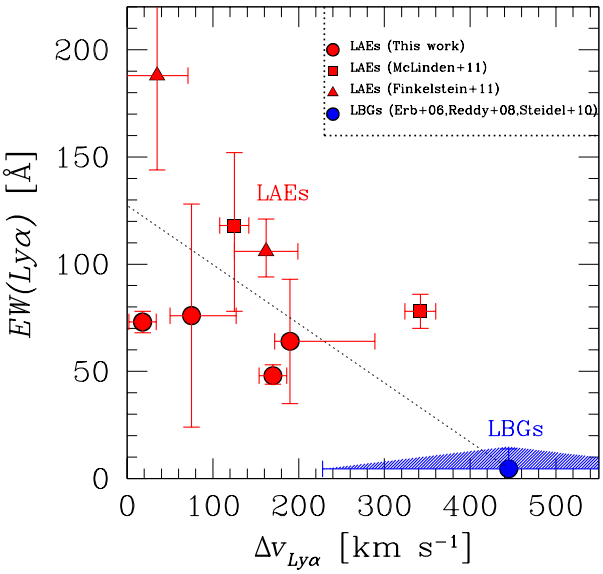


FIG. 7.— $\Delta v_{\rm Ly\alpha}$ as a function of rest-frame Ly$\alpha$ EW. The red square and triangle symbols show LAEs studied by McLinden et al. (2011) and Finkelstein et al. (2011), respectively. The blue symbol indicates the average $\Delta v_{\rm Ly\alpha}$ of 41 LBGs whose error bar represents 68 percentile of the $\Delta v_{\rm Ly\alpha}$ distribution (Steidel et al. 2010) and the average EW and its 68-percentile distribution (Reddy et al. 2008). The dotted line is the best-fit linear function to the data points.

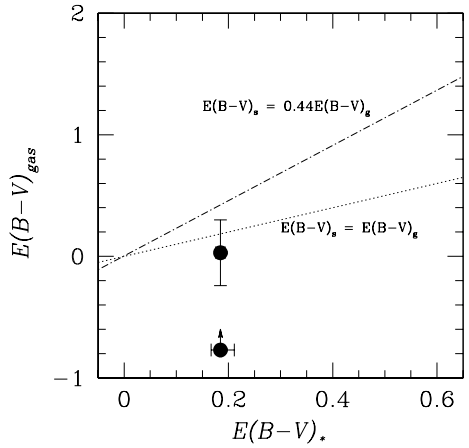


FIG. 8.— $E(B-V)_*$ and $E(B-V)_{gas}$ of our LAEs with a Balmer decrement measurement. The dotted and dashed lines show the relations of $E(B-V)_* = E(B-V)_{gas}$ (Erb et al. 2006b) and $E(B-V)_* = 0.44E(B-V)_{gas}$ (Calzetti et al. 2000), respectively.

value from our SED fitting. Similarly, the CDFS-6482's lower limit of $E(B-V)_{gas}$ is consistent with its $E(B-V)_*$. Thus, hereafter, we assume $E(B-V) \equiv E(B-V)_{gas} \simeq E(B-V)_*$ as proposed by Erb et al. (2006b) for starbursting galaxies.

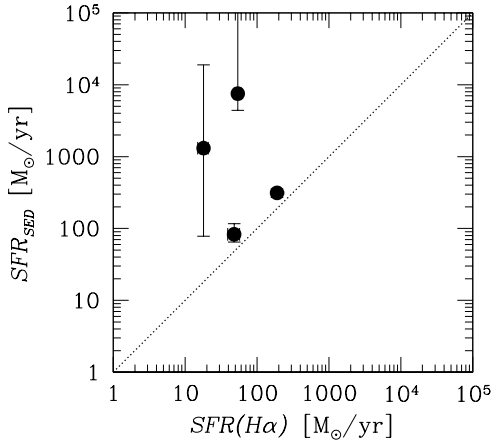


FIG. 9.— SFRs from SED fitting and H$\alpha$ luminosity for our LAEs. The circles denote COSMOS-13636, CDFS-6482, COSMOS-30679, and CDFS-3865, respectively, from left to right.

### 4.3. *Star Formation Rate*

An H$\alpha$ luminosity is thought to be a reliable indicator of SFR. We calculate SFRs of our LAEs from their dust-corrected H$\alpha$ luminosities using Kennicutt (1998)'s formula:

$$SFR(M_\odot\ \mathrm{yr}^{-1}) = 7.9\times10^{-42} L(\mathrm{H}\alpha)\ (\mathrm{erg\ s}^{-1}), \quad (4)$$

where Salpeter IMF is assumed. We obtain $SFR = 190\pm13 M_\odot$ yr$^{-1}$ (CDFS-3865), $48\pm9 M_\odot$ yr$^{-1}$ (CDFS-6482), $18\pm3 M_\odot$ yr$^{-1}$ (COSMOS-13636), and $54\pm6 M_\odot$ yr$^{-1}$ (COSMOS-30679). These SFRs are comparable to two $z = 2.2$ LAEs of Finkelstein et al. (2011), $36.8\pm5.8 M_\odot yr^{-1}$ and $23.6\pm6.5 M_\odot yr^{-1}$, estimated with H$\alpha$ emission. On the other hand, these SFRs are larger than the average values of $z\sim2.2$ LAEs obtained by the stacking analyses, $10-20 M_\odot$ yr$^{-1}$ (Nilsson et al. 2011; Nakajima et al. 2012). This difference is reasonable, because LAEs with an H$\alpha$ detection are generally brighter than those of average LAEs.

Figure 9 plots SFRs from SED fitting results and H$\alpha$ luminosities. Although these two estimates of SFRs are comparable for CDFS-3865 and CDFS-6482, these SFRs are largely different for COSMOS-13636 and COSMOS-30679. The large differences of SFRs in COSMOS-13636 and COSMOS-30679 indicate that models with very different star formation histories can fit the observed SED almost equally well. This figure thus demonstrates the importance of H$\alpha$ luminosity measurements for a reliable SFR. In the rest of this paper, we quote the SFRs estimated from H$\alpha$ emission.

### 4.4. *Ly$\alpha$ Escape Fraction*

Ly$\alpha$ escape fraction of a galaxy, $f_{esc}^{Ly\alpha}$, is defined as a ratio of Ly$\alpha$ photons escaping from the galaxy. This quantity can be a probe of the distribution and kinematics of inter-stellar medium (ISM). For example, outflowing ISM would make $f_{esc}^{Ly\alpha}$ larger since the number of resonant scattering and thus the chance of absorption by dust are reduced (e.g., Kunth et al. 1998; Atek et al. 2008).

Similarly, a clumpy distribution of ISM would also make $f_{esc}^{Ly\alpha}$ larger (e.g., Hansen & Oh 2006; Finkelstein et al. 2008).

Assuming the Case B recombination where the intrinsic ratio of Ly$\alpha$/H$\alpha$ is 8.7 (Brocklehurst 1971), we estimate the Ly$\alpha$ escape fraction from the observables as:

$$f_{esc}^{Ly\alpha} \equiv \frac{L_{obs}(Ly\alpha)}{L_{int}(Ly\alpha)} = \frac{L_{obs}(Ly\alpha)}{8.7 L_{int}(H\alpha)}, \quad (5)$$

where subscripts 'int' and 'obs' refer to intrinsic and observed quantities, respectively, and $L_{int}(H\alpha)$ is obtained by correcting the observed H$\alpha$ luminosity for dust extinction. Note that these $f_{esc}^{Ly\alpha}$ values are not measurements but estimates, because we assume the Case B recombination.

We find $f_{esc}^{Ly\alpha} = 0.14 \pm 0.03$ (CDFS-3865), $0.29 \pm 0.20$ (CDFS-6482), $0.57 \pm 0.13$ (COSMOS-13636), and $0.12 \pm 0.02$ (COSMOS-30679). These values are much higher than the average value of $z \sim 2$ star-forming galaxies, $\sim 5\%$ (Hayes et al. 2010). It is interesting because our LAEs have relatively large $E(B-V)$ values (Table 5). This would suggest that some mechanisms allow Ly$\alpha$ photons to escape from moderately dusty ISM (Atek et al. 2008). The upper left panel of Figure 13 presents $\Delta\ v_{Ly\alpha}$ vs. $f_{esc}^{Ly\alpha}$. Similar to Figure 7, it is possible that $f_{esc}^{Ly\alpha}$ anti-correlates with $\Delta\ v_{Ly\alpha}$.

### 4.5. *Size of our LAEs*

Assuming that stars dominate the total mass of the luminous (i.e., H$\alpha$ emitting) part of galaxies, we infer the size of our objects from the virial theorem as:

$$r = G\frac{M_*}{\sigma_v(H\alpha)^2} \sim 4.3\times10^{-6} \times \frac{M_*/M_\odot}{(\sigma_v(H\alpha)/kms^{-1})^2}(kpc), \quad (6)$$

where $M_*$ is the stellar mass and $\sigma_v(H\alpha)$ is the velocity dispersion measure from the H$\alpha$ line. Note that we divide the value by $10^{-5}$ for the scaling. We obtain $r = 1.1^{+0.1}_{-0.1}$ kpc (CDFS-3865), $5.0^{+1.1}_{-0.8}$ kpc (CDFS-6482), $9.0^{+1.8}_{-4.8}$ kpc (COSMOS-13636), and $107.5^{+35.6}_{-31.6}$ kpc (COSMOS-30679). Similarly, we derive sizes for 20 LBGs of Erb et al. (2006b) which have measurements of stellar mass and H$\alpha$ velocity dispersion. Here we multiply the stellar mass of Erb's sample by 1.8, since they assume a different IMF of Chabrier IMF (Chabrier 2003). Figure 10 plots the size and the stellar mass for our objects and those of Erb et al. (2006b). Interestingly, both the LAEs and the LBGs lie on the same power-law relation. In other words, less-massive galaxies of LAEs are smaller in size than more-massive galaxies of LBGs. Note that our LAEs are more massive than typical LAEs, so typical LAEs are probably even smaller than our LAEs.

## 5. DISCUSSION

### 5.1. $\Delta\ v_{Ly\alpha}$ *and Gas Motion of LAEs*

Due to the resonant nature of Ly$\alpha$, the observed Ly$\alpha$ line of a galaxy has a complicated profile depending on the kinematics and geometry of the ISM. A Ly$\alpha$ source in a simple static gas cloud produces a symmetric double-peaked profile centered at 1216Å due to significant resonance scattering at 1216Å(Harrington 1973; Neufeld 1990; Dijkstra et al. 2006). If the bluer peak is heavily absorbed by the intervening IGM along the line of sight, only the redder peak will be observed. Verhamme et al. (2006) have explained some of the observed Ly$\alpha$ profiles with a strong red peak and a weak blue peak with models of an expanding shell that absorbs Ly$\alpha$ photons at around 1216Å, although the surface brightness distribution may not be explained by such wind shells (see e.g., Barnes & Haehnelt 2009). Ly$\alpha$ emission line should show an asymmetric profile similar to a P Cygni profile in the case of outflow, while a symmetric double-peaked profile (or a nearly symmetric single red peak in the case with strong IGM absorption) is expected for the static gas cloud case (see Dijkstra et al. 2006; Harrington 1973; Neufeld 1990).

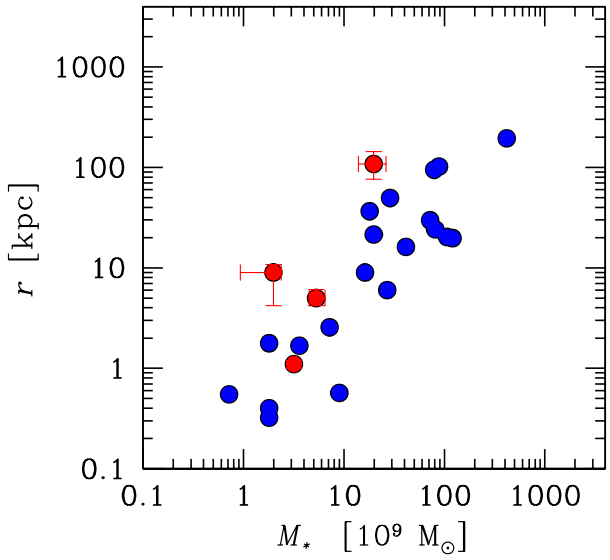


FIG. 10.— Stellar mass as a function of $r$. The red circles denote our LAEs, while the blue circles represent LBGs (Erb et al. 2006b; Steidel et al. 2010). We select 20 out of 114 LBGs which have reliable measurements of stellar mass and H$\alpha$ velocity dispersion.

To quantify the asymmetry of the Ly$\alpha$ line of our objects, we use the weighted skewness, $S_w$ (Kashikawa et al. 2006). The skewness is the third moment of the flux distribution, and the weighted skewness is defined as the product of the skewness and the line width. We obtain $S_w = 6.03 \pm 0.51$ (CDFS-3865), $5.45 \pm 1.59$ (CDFS-6482), $1.01 \pm 0.76$ (COSMOS-13636), and $5.31 \pm 4.06$ (COSMOS-30679) [14]. In the study of $z = 6.5$ LAEs, Kashikawa et al. (2006) classify emission lines with $S_w \geq 3$ as Ly$\alpha$ at $z = 6.5$ and those below $S_w = 3$ as low-$z$ nebular lines. Due to the redshift-dependent definition of $S_w$, an LAE with $S_w = 3$ at $z = 6.5$ have $S_w = 1.28$ if it is placed at $z = 2.2$. We find that all but COSMOS-13636 satisfy $S_w \geq 1.28$, although COSMOS-30679 has a large error because of the relatively noisy spectral profile. Although not meeting this criterion, COSMOS-13636 also has a positive $S_w$, possi-

[14] The $S_w$ of COSMOS-30679 is calculated after masking the wavelength range affected by the cosmic ray.

bly suggesting the line to be asymmetric. In either case, we cannot discriminate between symmetry and asymmetry for this object. We thus conclude that, at least, three out of the four LAEs with a large $S_w$ have an asymmetric Ly$\alpha$ line. These $S_w$ measurements indicate that the Ly$\alpha$ emission of our objects is mostly not originated from a static gas cloud but from outflowing gas.

If $\Delta v_{\rm Ly\alpha}$ values positively correlate with the speed of outflow, LAEs have a weaker outflow than LBGs. There is a hypothesis that Ly$\alpha$ photons can escape more easily with a larger outflow velocity, due to the reduced numbers of resonant scattering (e.g. Shapley et al. 2003). If this is the case, we should find a positive correlation between the outflow velocity and the Ly$\alpha$ EW. However, Figure 7 indicates the opposite tendency. The anti-correlation between the outflow velocity and the Ly$\alpha$ EW would rule out the hypothesis that outflow is the physical origin of very large Ly$\alpha$ EW objects.

Using simulations of Ly$\alpha$ radiative transfer in outflowing galaxies, Verhamme et al. (2006, 2008) suggest that not only IS absorption lines but also Ly$\alpha$ spectra are used to estimate the outflow velocity. In their simulations, they assume that a galaxy is surrounded by a spherically symmetric shell-like gas cloud in which HI gas and dust are well mixed. They also find that $\Delta v_{\rm Ly\alpha}$ tends to overestimate the expanding shell velocity, $v_{exp}$, in a high neutral hydrogen column density, $N$(HI). If a galaxy has a relatively small H I column density ($N$(HI)$< 10^{20}$ cm$^2$), the peak of Ly$\alpha$ profile emerges near the expanding velocity, $\Delta v_{\rm Ly\alpha} \approx v_{\rm exp}$. If, on the other hand, a galaxy has a high H I column density ($N$(HI)$> 10^{20}$ cm$^2$), the peak is offset by twice the expansion velocity, $\Delta v_{\rm Ly\alpha} \approx 2v_{\rm exp}$. Therefore, $\Delta v_{\rm Ly\alpha}$ may overestimate the expanding velocity up to a factor of $\sim 2$ for objects with a very high HI column density. However, the velocity offsets of our objects would correlate with the outflow velocity within a factor of 2 uncertainty.

In Section 4.1, we find that the average $\Delta v_{\rm Ly\alpha}$ of LAEs is $145^{+45}_{-23}$ km s$^{-1}$, significantly smaller than that of LBGs ($\simeq$ 400 km s$^{-1}$) at the same redshift. This observational result is important not only for understanding physical origin of Ly$\alpha$ emission in galaxies, but also for probing cosmic reionization with LAEs. If LAEs at $z > 6$ have a similarly small $\Delta v_{\rm Ly\alpha}$ value, some reionization models would need to revise the amount of Ly$\alpha$ photons scattered by inter-galactic medium (IGM). For example, Santos (2004) show the cases of $\Delta v_{\rm Ly\alpha} = 0$ and 360 km $^{-1}$, the latter of which is comparable to the average $\Delta v_{\rm Ly\alpha}$ of $z = 2 - 3$ LBGs. Recent reionization studies use Ly$\alpha$ emission of galaxies escaping from IGM as a probe of neutral hydrogen in the IGM (e.g. Kashikawa et al. 2006; Ota et al. 2008; Ouchi et al. 2010; Kashikawa et al. 2011). These studies assume the case of $\Delta v_{\rm Ly\alpha} = 360$ km $^{-1}$ for a realistic galaxy model to estimate neutral hydrogen fraction of IGM, $x_{\rm HI}$. If $z > 6$ LAEs have a small $\Delta v_{\rm Ly\alpha}$ value of $\simeq 145$ km s$^{-1}$, the previous estimates of $x_{\rm HI}$ from LAEs may be overestimated. Similarly, Ono et al. (2012); Schenker et al. (2012); Pentericci et al. (2011) find a significant drop of Ly$\alpha$ emitting galaxy fraction from $z \sim 6$ to 7. The derived $x_{\rm HI}$ value is as large as $\sim 40 - 60\%$. If this is true, the reionization takes place at the very late epoch, which cannot be easily explained by the large value of Thomson scattering optical depth, $\tau = 0.09$, obtained by WMAP observations (Dunkley et al. 2009; Komatsu et al. 2011). Future Ly$\alpha$ emitter models of reionization studies would need to implement our result of small average $\Delta v_{\rm Ly\alpha}$ value for the case that Ly$\alpha$ velocity offset does not significantly evolve over the cosmic time.

### 5.2. *Correlations Between the Outflow Velocity and the Physical Properties*

#### 5.2.1. *Outflow Velocity and SFR*

We examine the correlation between the outflow velocity and the SFR for the LAE and LBG samples in Figure 11. For the present-day universe, Martin (2005) have found in their sample of ULIRGs, LIRGs, and starburst dwarfs that those with larger outflow velocities, $v_{\rm out}$, tend to have higher SFRs, roughly following a power-law of $v_{\rm out} \propto SFR^{0.35}$. This correlation implies that galaxies with a high SFR tend to have more massive stars and supernovae (SNe) which drive an outflow. As pointed out by some authors (e.g. Martin 2005; Steidel et al. 2010), this correlation is found only for galaxies with a SFR of $\gtrsim 10 - 100 M_\odot yr^{-1}$.

Figure 11 indicates that there may exist a positive correlation between $\Delta v_{\rm Ly\alpha}$ and SFR for our LAEs, although the statistics is not very good. For comparison, we also plot $\sim 30$ LBGs taken from the literature (Erb et al. 2006b; Steidel et al. 2010); a positive but a flatter correlation is found. It is thus found that LAEs and LBGs do not follow the same power law, and that LAEs have systematically smaller outflow velocities at a given SFR. Theoretically, the slope of the correlation depends on the dominant physical process of outflow (Kornei et al. 2012). A linear correlation, $v_{\rm out} \propto SFR$, is expected for radiation pressure dominant outflow (Sharma et al. 2011), while shallower slopes are indicative of ram pressure dominant outflow (Heckman et al. 2000). Because the LAEs show a linear correlation of $v_{\rm out} \propto SFR$ in Figure 11, outflows in LAEs would be driven by radiation pressure.

#### 5.2.2. *Outflow Velocity and $\sigma_v(H\alpha)$*

We then examine how the outflow velocity correlates with the H$\alpha$ velocity dispersion, $\sigma_v(H\alpha)$, which is related to the gravitational potential of the galaxy. Martin 2005 have found that the terminal outflow velocity always approaches the galactic escape velocity, which is consistent with a theoretical prediction (e.g., Murray et al. 2005). The middle panel of Figure 11 presents $\Delta v_{\rm Ly\alpha}$ as a function of $\sigma_v(H\alpha)$ for our LAEs, together with those of $\sim 20$ LBGs (Erb et al. 2006b; Steidel et al. 2010). It is not clear whether there exists a correlation with the given poor statistics and large errors. However, it is obvious that LAEs have smaller outflow velocities than LBGs at a given $\sigma_v(H\alpha)$.

#### 5.2.3. *Outflow Velocity and SFR density*

Finally, we investigate the outflow velocity correlation with the SFR density ($\Sigma_{SFR}$) which represents the intensity of star forming activity. The right panel of Figure 11 plots $\Sigma_{SFR}$ and $\Delta v_{\rm Ly\alpha}$ for our LAEs and the LBGs in the literature. Here we estimate $\Sigma_{SFR}$ by dividing the SFR by the size derived in §4.5. The $\Sigma_{SFR}$ values of our objects are $157^{+31}_{-31}$ M$_\odot$ yr$^{-1}$ kpc$^{-2}$ (CDFS-3865), $1.9^{+0.9}_{-0.7}$ M$_\odot$ yr$^{-1}$ kpc$^{-2}$ (CDFS-6482), $0.22^{+0.096}_{-0.22}$ M$_\odot$ yr$^{-1}$ kpc$^{-2}$(COSMOS-13636), and $4.67^{+3.13}_{-2.80} \times 10^{-3}$ M$_\odot$ yr$^{-1}$ kpc$^{-2}$(COSMOS-30679). [15] LAEs have a small $\Delta v_{\rm Ly\alpha}$ at a given $\Sigma_{SFR}$. This result implies that the physical origin of LAE outflows would be different from that of LBG outflows.

### 5.3. *Why LAEs Have Strong Ly$\alpha$ Emission?*

In this subsection, we discuss the physical origin of strong Ly$\alpha$ emission from LAEs. There are various possibilities of

[15] Although many studies have adopted the Petrosian radius for the size, it is known that the Petrosian radius is likely to overestimate the size of star forming regions especially for high-$z$ galaxies which have clumpy star forming regions (Kornei et al. 2012).

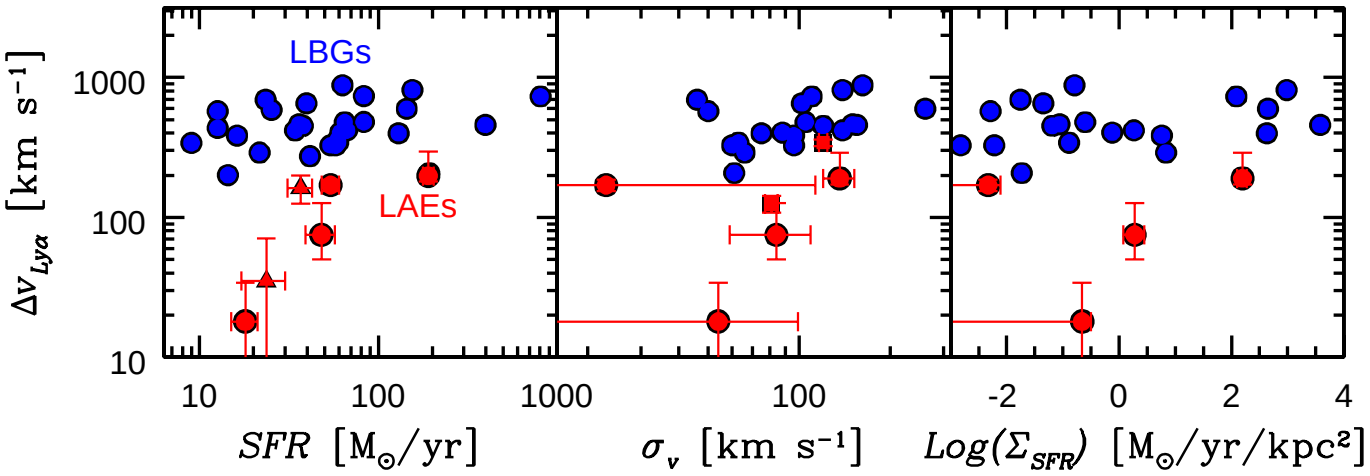


FIG. 11.— $\Delta\, v_{Ly\alpha}$ as a function of SFR (left panel), $\sigma_v(H\alpha)$ (middle panel), and $\Sigma_{SFR}$ (right panel). For all panels, the red circles represent our LAEs. Red triangles in the left panel denote LAEs at $z \sim 2.3$ (Finkelstein et al. 2011). Red squares in the middle panel indicate LAEs at $z \sim 3$ (McLinden et al. 2011).

strong Ly$\alpha$ emission; shock heating of outflow, very weak dust extinction, and geometry of dust/gas clouds. In the following subsections, we examine the weak-dust hypothesis and the clumpy-cloud hypothesis.

#### 5.3.1. *Weak Dust Extinction*

It is possible that Ly$\alpha$ photons survive through resonance scattering in gas clouds with little dust. In this case, one should find significantly small $E(B-V)$ in LAEs and a negative correlation between $E(B-V)$ and Ly$\alpha$ EW. The middle panels of Figure 13 plot $E(B-V)$ as a function of EW(Ly$\alpha$) and $f_{esc}^{Ly\alpha}$. There is no significant correlation in either panel. Hayes et al. (2010) and Kornei et al. (2010) have reported an anti-correlation between $f_{esc}^{Ly\alpha}$ and $E(B-V)$ in their H$\alpha$ emitters (HAEs) at $z \sim 2.2$. However, in our $f_{esc}^{Ly\alpha}$ vs $E(B-V)$ plot, there are objects with relatively high $f_{esc}^{Ly\alpha}$ of $0.4-0.7$ even in a moderately high extinction of $E(B-V) = 0.2-0.3$. Therefore, it is not clear if weak dust extinction solely can explain the strong Ly$\alpha$ emission.

#### 5.3.2. *Clumpy Cloud Hypothesis*

The gas distribution in LAEs may not be smooth and spherically symmetric, but clumpy. In a clumpy geometry, dust grains are shielded by HI gas, and Ly$\alpha$ photons are resonantly scattered on the surface of the ISM without being absorbed by dust (Neufeld 1991; Hansen & Oh 2006). Because continuum photons are absorbed through dusty gas clouds, the ratio of Ly$\alpha$ to UV continuum fluxes, or Ly$\alpha$ EW, is enhanced. For further discussion of the clumpy cloud hypothesis, we calculate the clumpiness parameter, $q$, introduced by Finkelstein et al. (2008):

$$q = \tau(Ly\alpha)/\tau_{1216}, \qquad (7)$$

where $\tau$(Ly$\alpha$) and $\tau_{1216}$ are defined as $e^{-\tau(\mathrm{Ly}\alpha)} = L_{\mathrm{obs}}(\mathrm{Ly}\alpha)/L_{\mathrm{int}}(\mathrm{Ly}\alpha)$ and $e^{-\tau_{1216}} = 10^{-0.4k_{1216}E(B-V)}$ with the extinction coefficient at $\lambda = 1216\mathring{A}$, $k_{1216} = 11.98$ (Calzetti et al. 2000). This parameter is used to diagnose the geometry of the ISM (e.g., Finkelstein et al. 2008; Kornei et al. 2010). If the geometry of the ISM is clumpy, $q$ is smaller than unity. In the case of $q > 1$, Ly$\alpha$ photons are more preferentially absorbed by dust through relatively homogeneous ISM.

The $q$ values of our objects are calculated to be $q = 0.96 \pm 0.11$ (CDFS-3865), $q = 0.61 \pm 0.34$ (CDFS-6482), $q = 0.19^{+0.07}_{-0.09}$ (COSMSO-13636), and $q = 0.36^{+0.03}_{-0.03}$ (COSMOS-30679); three of the four objects clearly have $q < 1$ beyond the uncertainties. These results are consistent with that of Nakajima et al. (2012) who obtained $q = 0.7^{+0.1}_{-0.1}$ for $z = 2.2$ stacked LAEs. On the other hand, some studies have found more LAEs with $q > 1$ at $z \sim 2$ (e.g., Nilsson et al. 2009; Hayes et al. 2010).

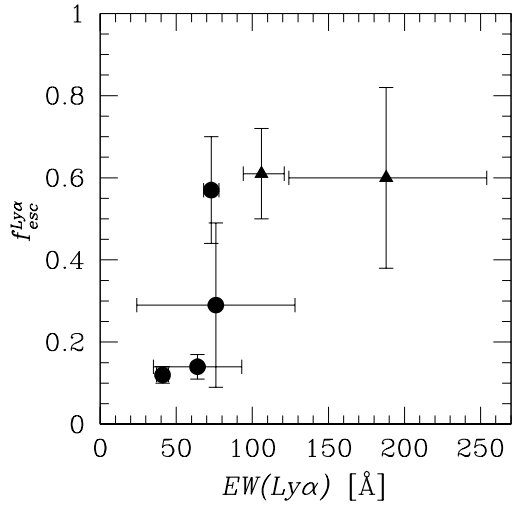


FIG. 12.— EW(Ly$\alpha$) as a function of $f_{esc}^{Ly\alpha}$. The circles indicate our objects, and the triangles represent $z \sim 2.3$ LAEs of Finkelstein et al. (2011).

The right panels of Figure 13 show $q$ as a function of $f_{esc}^{Ly\alpha}$ and Ly$\alpha$ EW, respectively, for the LAEs sample. There may exist a negative correlation between $q$ and $f_{esc}^{Ly\alpha}$, although it is not very clear due to the poor statistics. More data are needed to uncover the physical origin of strong Ly$\alpha$ emission. However, from the discussions in Section 5.1, a simple picture of outflow and Ly$\alpha$ escape does not seem to be the primary reason for the strong Ly$\alpha$ emission of LAEs.

## 6. CONCLUSIONS

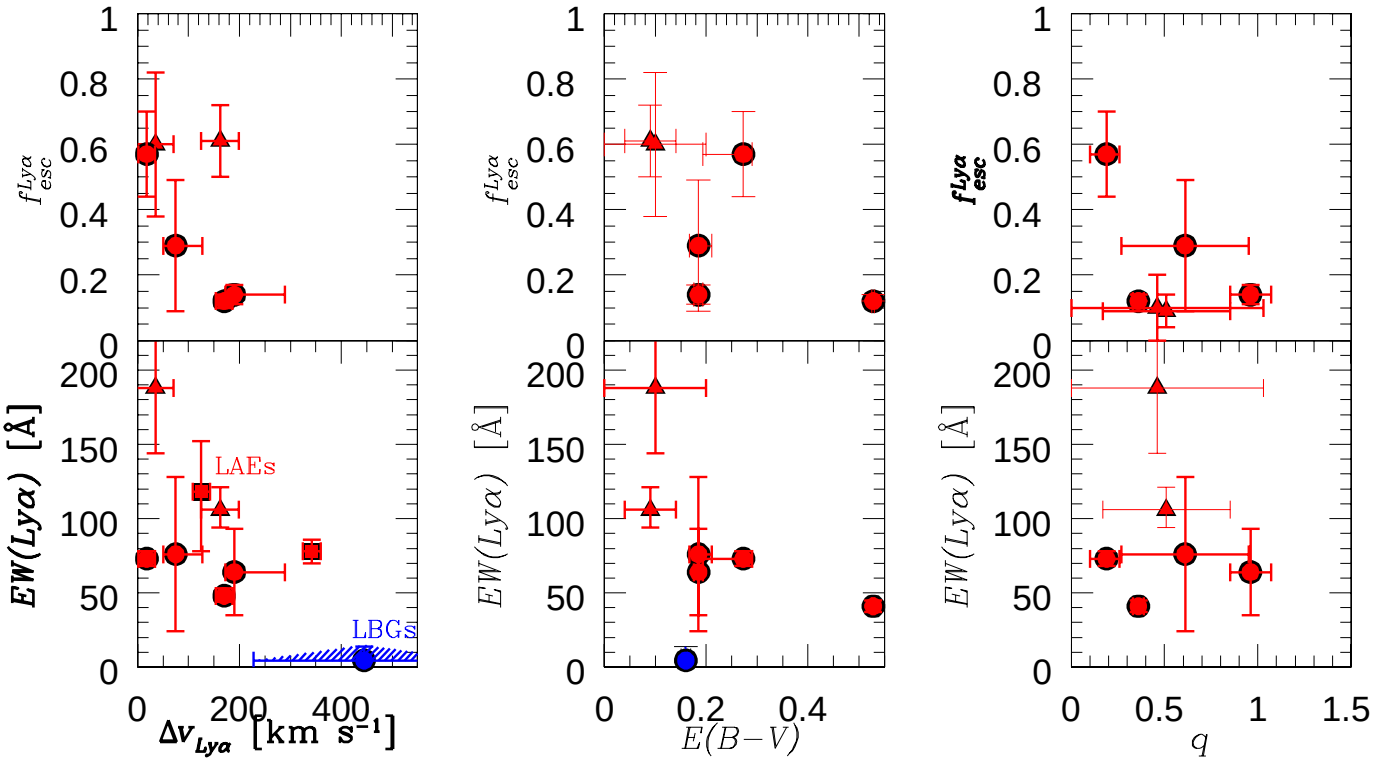


FIG. 13.— $\Delta\, v_{Ly\alpha}$, $E(B-V)$, and $q$ plotted against $f_{esc}^{Ly\alpha}$ and EW(Ly$\alpha$). The red circles denote our LAEs, and the green and magenta circles are LAEs given by McLinden et al. (2011) and Finkelstein et al. (2011), respectively. The blue circles represent LBGs (Erb et al. 2006b; Reddy et al. 2008; Steidel et al. 2010).

TABLE 6
SUMMARY OF THE PHYSICAL QUANTITIES

| Object | $E(B-V)_*$ (1) | $M_*$ $10^9$ M$_\odot$ (2) | $EW(Ly\alpha)$ Å (3) | $\Delta v_{Ly\alpha}$ km s$^{-1}$ (4) | $L(H\alpha)$ $10^{41}$ erg s$^{-1}$ (5) | $\sigma_v(H\alpha)$ km s$^{-1}$ (6) | $SFR(H\alpha)$ M$_\odot$ yr$^{-1}$ (7) | $f_{esc}^{Ly\alpha}$ (8) | $r$ kpc (9) | $q$ (10) |
|---|---|---|---|---|---|---|---|---|---|---|
| CDFS-3865 | $0.185^{+0.009}_{-0.009}$ | $3.18^{+0.21}_{-0.13}$ | $64^{+29}_{-29}$ | $190^{+99}_{-18}$ | $136.5^{+8.5}_{-8.5}$ | 110.8 | $190^{+13}_{-13}$ | $0.14^{+0.03}_{-0.03}$ | $1.1^{+0.1}_{-0.1}$ | $0.96^{+0.11}_{-0.11}$ |
| CDFS-6482 | $0.185^{+0.026}_{-0.018}$ | $5.30^{+1.18}_{-0.80}$ | $76^{+52}_{-52}$ | $75^{+52}_{-25}$ | $34.5^{+6.2}_{-6.2}$ | 67.5 | $48^{+9}_{-9}$ | $0.29^{+0.20}_{-0.20}$ | $5.0^{+1.1}_{-0.8}$ | $0.61^{+0.34}_{-0.34}$ |
| COSMOS-13636 | $0.273^{+0.018}_{-0.079}$ | $1.99^{+0.39}_{-1.06}$ | $73^{+5}_{-5}$ | $18^{+16}_{-16}$ | $9.5^{+1.3}_{-1.3}$ | 30.7 | $18^{+3}_{-3}$ | $1.99^{+0.39}_{-1.06}$ | $9.0^{+1.8}_{-4.8}$ | $0.19^{+0.07}_{-0.09}$ |
| COSMOS-30679 | $0.528^{+0.0026}_{-0.0026}$ | $19.75^{+6.53}_{-5.80}$ | $41^{+4}_{-4}$ | $170^{+16}_{-16}$ | $24.2^{+2.1}_{-2.1}$ | 28.1 | $54^{+6}_{-6}$ | $0.12^{+0.02}_{-0.02}$ | $107.5^{+35.6}_{-31.6}$ | $0.36^{+0.03}_{-0.03}$ |

Notes. (1) Dust extinction estimated from the SED fitting; (2) Stellar mass estimated from the SED fitting; (3) Rest-frame Ly$\alpha$ EW; (4) Velocity offset of the Ly$\alpha$ line; (5) H$\alpha$ luminosity; (6) Velocity dispersion of H$\alpha$ line; (7) Star formation rate from H$\alpha$ luminosity corrected for dust extinction; (8) Ly$\alpha$ escape fraction estimated in §4.4; (9) Size of a galaxy derived in §4.5 under the assumption that stars dominate a total mass of luminous component of galaxy; (10) Clumpiness parameter (§5.3.2).

We have presented the results of Magellan/MMIRS and Keck/NIRSPEC spectroscopic observations of five Ly$\alpha$ emitters (LAEs) at $z \sim 2.2$ which are taken from the sample of K. Nakajima et al. (in preparation; see Nakajima et al. 2012 for the selection). This redshift is unique since we can observe both Ly$\alpha$ and nebular emission lines from the ground. We have successfully detected H$\alpha$ emission from all five objects, and [OII] $\lambda\lambda$3726, 3729, H$\beta$, and/or [OIII] $\lambda\lambda$4959, 5007 for some LAEs. After removing an AGN-contaminated object, we have measured the velocity offset of Ly$\alpha$ line from the systemic redshift determined by nebular emission lines to discuss the gas motion statistics of LAEs. The major results of our study are summarized below.

- We find that Ly$\alpha$ is redshifted with respect to the systemic redshift by $\Delta v_{\rm Ly\alpha} = 190^{+99}_{-18}$ km$^{-1}$ (CDFS-3865), $75^{+52}_{-25}$ km$^{-1}$ (CDFS-6482), $18 \pm 16$ km$^{-1}$ (COSMOS-13636), and $170 \pm 16$ km$^{-1}$ (COSMOS-30679). Combining the four LAEs from the literature, we find that LAEs have an average of $\Delta v_{\rm Ly\alpha} = 145^{+45}_{-23}$km s$^{-1}$ which is systematically smaller than those of BX/BM LBGs at $z \sim 2-3$, $\Delta v_{\rm Ly\alpha} \simeq 400$ km s$^{-1}$. This finding affects some reionization studies, since they assume a medium high velocity of $\Delta v_{\rm Ly\alpha} \simeq 400$km s$^{-1}$ to estimate the neutral hydrogen fraction of the IGM, $x_{\rm HI}$. If $z > 6$ LAEs have $\Delta v_{\rm Ly\alpha}$ values as small as $145^{+45}_{-23}$ km s$^{-1}$, $x_{\rm HI}$ of these previous studies with LAEs may be overestimated.

- There is an anti-correlation between Ly$\alpha$ EW and $\Delta v_{\rm Ly\alpha}$ in the compilation of the LAE and LBG samples. In other words, a galaxy with stronger Ly$\alpha$ emission has a smaller $\Delta v_{\rm Ly\alpha}$. Because our LAEs have a positive $\Delta v_{\rm Ly\alpha}$ velocity of Ly$\alpha$ emission whose profiles

are asymmetric with a weighted skewness of $S_w > 1.28$, it is implied that our LAEs have outflowing gas whose velocity would correlate with $\Delta v_{\rm Ly\alpha}$. It is likely that LAEs have a smaller outflow velocity than LBGs. However, the anti-correlation indicates that a simple picture of outflow+Ly$\alpha$ escape may not be able to explain the strong Ly$\alpha$ emission of LAEs.

- To investigate the physical origin that LAEs likely have small outflow velocities than LBGs, we have examined the relation between the outflow velocity and three physical parameters: $SFR$, $\Sigma_{SFR}$, and $\sigma(H\alpha)$. Because LAEs would follow a linear relation of $v_{\rm out} \propto SFR$, the outflow of LAEs may be driven by the radiation pressure. Because LAEs have smaller outflow velocities than LBGs with similar $SFR$, $\Sigma_{SFR}$, and $\sigma(H\alpha)$, there may exist a physical event that produces strong Ly$\alpha$ emission in similar galaxies.
- We have shown that $f_{esc}^{Ly\alpha}$ is weakly anti-correlated with $\Delta v_{\rm Ly\alpha}$. We have also found that there is no significant correlation between Ly$\alpha$ EW and $E(B-V)$. It is not clear if the weak dust solely can explain the high escape fraction of Ly$\alpha$ photons. Finally, there may exist an anti-correlation between $f_{esc}^{Ly\alpha}$ and the clumpiness parameter, $q$. More data and theoretical work are needed to uncover the physical origin of strong Ly$\alpha$ emission.

ACKNOWLEDGEMENTS

We thank Kentaro Motohara and Masakazu Kobayashi for their helpful comments. We acknowledge Brian McLeod and Paul Martini who gave us helpful advices on our MMIRS observations and data reduction. We are grateful to Magellan and Keck Telescope staff for supporting our MMIRS and NIRSPEC observations. This work was supported by KAKENHI (23244025) Grant-in-Aid for Scientific Research(A) through Japan Society for the Promotion of Science (JSPS), and NSF grant 1108815 awarded by National Science Foundation.

REFERENCES

Atek, H., Kunth, D., Hayes, M., Östlin, G., & Mas-Hesse, J. M. 2008, A&A, 488, 491
Baldwin, J. A., Phillips, M. M., & Terlevich, R. 1981, PASP, 93, 5
Barnes, L. A., & Haehnelt, M. G. 2009, MNRAS, 397, 511
Bond, N. A., Feldmeier, J. J., Matković, A., Gronwall, C., Ciardullo, R., & Gawiser, E. 2010, ApJ, 716, L200
Bond, N. A., Gawiser, E., Gronwall, C., Ciardullo, R., Altmann, M., & Schawinski, K. 2009, ApJ, 705, 639
Brocklehurst, M. 1971, MNRAS, 153, 471
Bruzual, G., & Charlot, S. 2003, MNRAS, 344, 1000
Calzetti, D., Armus, L., Bohlin, R. C., Kinney, A. L., Koornneef, J., & Storchi-Bergmann, T. 2000, ApJ, 533, 682
Cardamone, C. N., et al. 2010, ApJS, 189, 270
Chabrier, G. 2003, PASP, 115, 763
Cowie, L. L., Barger, A. J., & Hu, E. M. 2011, ApJ, 738, 136
Dekel, A., et al. 2009, Nature, 457, 451
Dijkstra, M., Haiman, Z., & Spaans, M. 2006, ApJ, 649, 14
Dunkley, J., et al. 2009, ApJS, 180, 306
Erb, D. K., Shapley, A. E., Pettini, M., Steidel, C. C., Reddy, N. A., & Adelberger, K. L. 2006a, ApJ, 644, 813
Erb, D. K., Steidel, C. C., Shapley, A. E., Pettini, M., Reddy, N. A., & Adelberger, K. L. 2006b, ApJ, 646, 107
Finkelstein, S. L., Papovich, C., Rudnick, G., Egami, E., Le Floc'h, E., Rieke, M. J., Rigby, J. R., & Willmer, C. N. A. 2009, ApJ, 700, 376
Finkelstein, S. L., Rhoads, J. E., Malhotra, S., Grogin, N., & Wang, J. 2008, ApJ, 678, 655
Finkelstein, S. L., et al. 2011, ApJ, 729, 140
Guaita, L., et al. 2011, ApJ, 733, 114
Hansen, M., & Oh, S. P. 2006, MNRAS, 367, 979
Harrington, J. P. 1973, MNRAS, 162, 43
Hayes, M., et al. 2010, Nature, 464, 562
Heckman, T. M., Armus, L., & Miley, G. K. 1990, ApJS, 74, 833
Heckman, T. M., Lehnert, M. D., Strickland, D. K., & Armus, L. 2000, ApJS, 129, 493
Kashikawa, N., et al. 2006, ApJ, 648, 7
—. 2011, ApJ, 734, 119
Kauffmann, G., et al. 2003, MNRAS, 346, 1055
Kelson, D. D. 2003, PASP, 115, 688
Kennicutt, Jr., R. C. 1998, ARA&A, 36, 189
Kewley, L. J., Dopita, M. A., Sutherland, R. S., Heisler, C. A., & Trevena, J. 2001, ApJ, 556, 121
Komatsu, E., et al. 2011, ApJS, 192, 18
Kornei, K. A., Shapley, A. E., Erb, D. K., Steidel, C. C., Reddy, N. A., Pettini, M., & Bogosavljević, M. 2010, ApJ, 711, 693
Kornei, K. A., Shapley, A. E., Martin, C. L., Coil, A. L., Lotz, J. M., Schiminovich, D., Bundy, K., & Noeske, K. G. 2012, ArXiv e-prints
Kunth, D., Mas-Hesse, J. M., Terlevich, E., Terlevich, R., Lequeux, J., & Fall, S. M. 1998, A&A, 334, 11
Larson, R. B. 1974, MNRAS, 169, 229
Madau, P. 1995, ApJ, 441, 18
Martin, C. L. 2005, ApJ, 621, 227
McCracken, H. J., et al. 2010, ApJ, 708, 202
McLinden, E. M., et al. 2011, ApJ, 730, 136
Murray, N., Quataert, E., & Thompson, T. A. 2005, ApJ, 618, 569
Nakajima, K., et al. 2012, ApJ, 745, 12
Neufeld, D. A. 1990, ApJ, 350, 216
—. 1991, ApJ, 370, L85
Nilsson, K. K., Östlin, G., Møller, P., Möller-Nilsson, O., Tapken, C., Freudling, W., & Fynbo, J. P. U. 2011, A&A, 529, A9
Nilsson, K. K., Tapken, C., Møller, P., Freudling, W., Fynbo, J. P. U., Meisenheimer, K., Laursen, P., & Östlin, G. 2009, A&A, 498, 13
Oke, J. B., & Gunn, J. E. 1983, ApJ, 266, 713
Ono, Y., et al. 2010, MNRAS, 402, 1580
—. 2012, ApJ, 744, 83
Osterbrock, D. E. 1989, Astrophysics of gaseous nebulae and active galactic nuclei, ed. Osterbrock, D. E.
Ota, K., et al. 2008, ApJ, 677, 12
Ouchi, M., et al. 2010, ApJ, 723, 869
Peng, C. Y., Ho, L. C., Impey, C. D., & Rix, H.-W. 2002, AJ, 124, 266
Pentericci, L., et al. 2011, ApJ, 743, 132
Pettini, M., Rix, S. A., Steidel, C. C., Adelberger, K. L., Hunt, M. P., & Shapley, A. E. 2002, ApJ, 569, 742
Rakic, O., Schaye, J., Steidel, C. C., & Rudie, G. C. 2011, MNRAS, 414, 3265
Reddy, N. A., Steidel, C. C., Pettini, M., Adelberger, K. L., Shapley, A. E., Erb, D. K., & Dickinson, M. 2008, ApJS, 175, 48
Salpeter, E. E. 1955, ApJ, 121, 161
Santos, M. R. 2004, MNRAS, 349, 1137
Schaerer, D., & de Barros, S. 2009, A&A, 502, 423
Schenker, M. A., Stark, D. P., Ellis, R. S., Robertson, B. E., Dunlop, J. S., McLure, R. J., Kneib, J.-P., & Richard, J. 2012, ApJ, 744, 179
Shapley, A. E., Steidel, C. C., Pettini, M., & Adelberger, K. L. 2003, ApJ, 588, 65
Sharma, M., Nath, B. B., & Shchekinov, Y. 2011, ApJ, 736, L27
Steidel, C. C., Erb, D. K., Shapley, A. E., Pettini, M., Reddy, N., Bogosavljević, M., Rudie, G. C., & Rakic, O. 2010, ApJ, 717, 289
Verhamme, A., Schaerer, D., Atek, H., & Tapken, C. 2008, A&A, 491, 89
Verhamme, A., Schaerer, D., & Maselli, A. 2006, A&A, 460, 397
Yang, Y., Zabludoff, A., Jahnke, K., Eisenstein, D., Davé, R., Shectman, S. A., & Kelson, D. D. 2011, ApJ, 735, 87